

# Examining Explicit Discretization in Spectral Schemes

## Supplemental Material

### Overview

This document includes additional details and results from the publication "Examining Explicit Discretization in Spectral Schemes". The contents have been separated into five appendices, each of which is summarized in the table of contents below. [Appendix A](#) and [Appendix B](#) provide details and discussions related to how we generated and, subsequently, numerically modeled the color maps we investigated. [Appendix C](#) justifies the methods employed to select bandwidths for the kernel density estimates in our analyses. [Appendix D](#) provides additional details regarding the descriptive statistics that we ran using the number of delimiters counted and placed by the study participants. Finally, [Appendix E](#) provides a comprehensive overview of results and analyses discussed in Sections 5 and 6 of the paper.

This document *does not* include the high-resolution figure versions, cleaned study data, or the study software also mentioned in the paper; each of those have been included separately within the archive containing this document. Additional details on those items can be found in the accompanying README file.

### Contents

#### [Appendix A The Kindlmann Color Map](#)

An expanded discussion of our decision to use the Kindlmann color map in the study, as referenced in Section 4.3 of the paper.

#### [Appendix B Indicator Derivation Process](#)

A detailed overview of the numerical methods used to derive the indicator sets used in our analyses, expanding on discussions from Sections 5.2.

#### [Appendix C Kernel Density Estimates and Dependent Data](#)

An examination of various potential issues with kernel density estimation (KDE) and how we have addressed them in this work.

#### [Appendix D Descriptive Statistical Analysis \(Expanded\)](#)

An expanded NHST style description of the statistical analysis of the number of delimiters participants counted and placed.

#### [Appendix E Results Overview \(Expanded\)](#)

The full set of participants' boundary placement results shown using the visual analysis methods employed in Sections 5 and 6 of the paper, along with an expanded discussion of the grayscale results.

### References

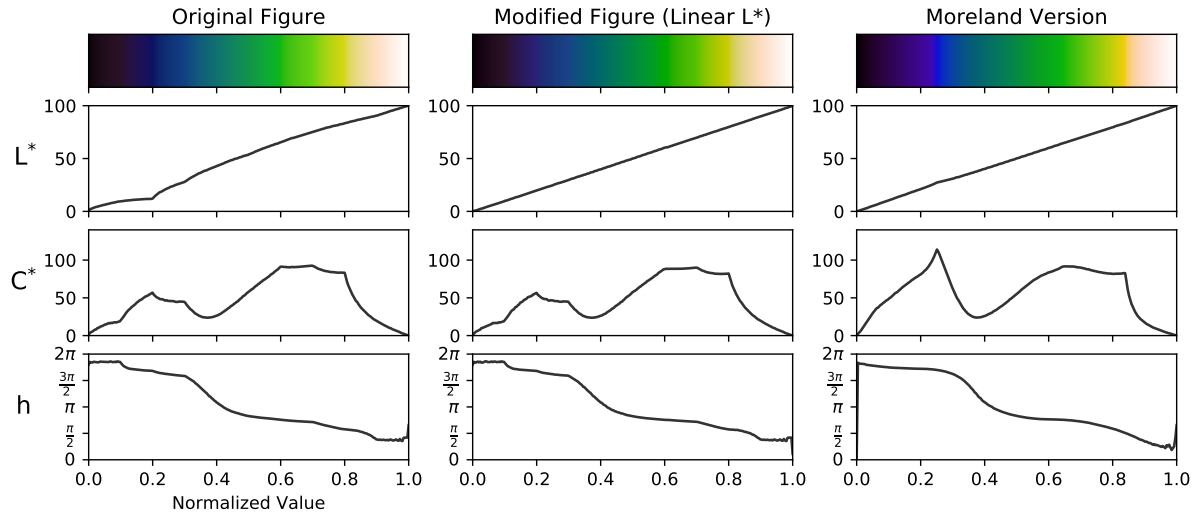


**Figure 1:** CIELCh profiles for three Kindlmann color map variants: the original paper version, the modified version used in our study, and Moreland’s version.

### A. The Kindlmann Color Map

The *Kindlmann* color map is one of two color maps introduced by Kindlmann et al. [KRC02] while outlining a novel method for quickly and individually controlling for perceived luminance in a device-dependent RGB color space. In the paper, Kindlmann et al. illustrate how their method can be used to take the control points of the traditional rainbow color map and create either an isoluminant rainbow or a rainbow color map that linearly increases in luminance. The latter, variations of which are shown in Figure 1, is colloquially referred to as the Kindlmann color map [Mor16, DPR\*18]. Although Kindlmann et al. never specifically advocated for people to use either of these color maps, both color maps have an established pattern of recognized use within the visualization community [Mor16, STP17, YLL15, ZH16, DPR\*18, CZC\*18].

The Kindlmann color map belongs to larger set of *spiral* color maps, which vary monotonically in luminance in order to accurately convey form information while simultaneously spiraling through a range of hues in order to reduce simultaneous contrast and improve value estimation [Mor16, War88]. Alternate examples of spiral color maps include the cubehelix [Gre11] and black body [Mor16] color maps. As stated in the paper, we settled on the Kindlmann color map, because it traverses a similar distribution of hue values to the traditional rainbow and jet color maps, and it exhibits clear banding effects that cannot be explained by luminance variation [DPR\*18].

Unfortunately, a widely accepted device-independent definition of the Kindlmann color map does not currently exist. The original color map presented by Kindlmann et al. was derived using individualized, device-dependent judgments made by one of the authors [KRC02]. Even though the color map was designed to vary linearly in perceived luminance, as Figure 1 shows, the lightness ( $L^*$ ) profile of the color map is not completely linear when evaluated in a perceptually uniform color space such as CIELAB or CIELCh. Niccoli proposes a practical solution of simply modify-

ing the color map to force the lightness profile to be linear [Nic12]. Moreland, on the other hand, attempted to programmatically define a device-independent version of the Kindlmann color map directly in CIELAB [Mor16].

Figure 1 illustrates the differences between the various versions of the Kindlmann color map in sRGB color space. On a monitor properly calibrated to display sRGB, Moreland’s version contains increasingly pronounced blue and yellow banding compared to the original version proposed by Kindlmann et al. A similar difference, however, is likely discernible in a wide variety of real-world viewing conditions (e.g., utilizing the device-dependent RGB of different monitors with different calibration settings under different lighting conditions) [Sza18], despite not being fully reflective of true CIELCh coordinates. In line with our H2 hypothesis, this difference appears to correspond to major differences in the underlying chroma ( $C^*$ ) profiles.

Although many of the papers that employ the Kindlmann color map do not specify what version of the color map they use [STP17, YLL15, DPR\*18], we opted to linearize the the luminance profile of the original paper version, following the general process outlined by Niccoli [Nic12]. We reconstructed the color map directly from the figure image included in the original paper, converted the color map to CIELAB, replaced the luminance profile with a linear ramp, and finally converted the result back to sRGB. The resulting color map reasonably approximates the original version and is straightforward to reproduce.

The downside of deriving the Kindlmann color map in this manner, however, is that the resulting color map contains a notable amount of noise in both its CIELCh chroma and hue profiles. As we discuss in Appendix B, the numerical methods employed to derive both cusps and inflection points within the CIELCh profiles are highly sensitive to noise, generating artifacts in our indicator set derivations.

## B. Indicator Derivation Process

Section 5.2 of the paper outlines the process we used to derive the locations of both cusps and inflection points from the CIELCh luminance, chroma, and hue profiles of the 4 color maps in the study. Since numerical approximations are known to be sensitive to noise [KC01], we begin by smoothing the values of the luminance, chroma, and hue profiles using a Gaussian, where the amount of smoothing is parameterized by  $\sigma$ . We then create cubic-spline interpolating polynomials that approximate those smoothed CIELCh profiles.

The locations of cusps are derived using the second and third derivatives of these interpolating polynomials. The roots of the third derivative provide the locations of local maxima/minima in the second derivative, which represents curvature. The absolute value of the second derivative provides curvature magnitude, which can be thresholded to find the set of local maxima/minima with arbitrarily high curvature magnitude, which represent cusps. Inflection points can be derived similarly, using the roots of the second derivative (i.e., locations of zero curvature) and thresholding based on gradient magnitude. This process is illustrated in Figure 5 of the paper, a modified version of which is reproduced in Figure 2 for convenience.

Smoothing and thresholding, however, can do only so much to reduce numeric artifacts. Figure 2 highlights that the derived set inflection points contain spurious indicators associated with boundary conditions and cusps, which are caused by approximating the chroma profile using a cubic-spline interpolating polynomial, which is fully continuous and differentiable everywhere. One could increase the thresholding parameter ( $\tau$ ) to eliminate these spurious indicators, but doing so would also eliminate real inflection points that we want to capture (e.g., the inflection points seen at approximately 0.63 and 0.91). Alternatively, one could try to increase the amount of smoothing ( $\sigma$ ) performed before generating the interpolating polynomial. Increasing smoothing too much, however, can alter the chroma profile significantly, raising questions about the

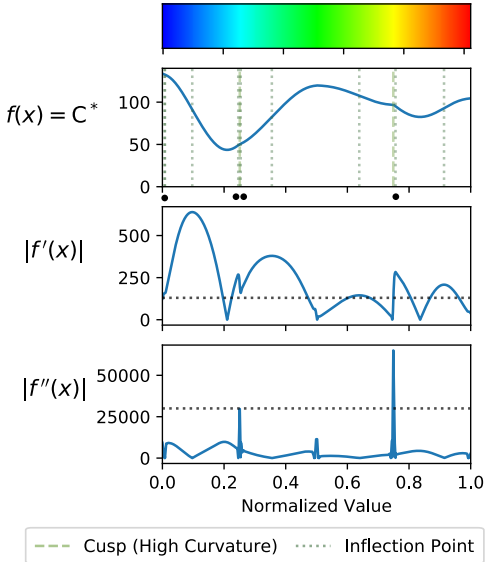


**Figure 2:** Deriving the chroma ( $C^*$ ) indicators for the traditional rainbow color map: (upper) the cubic spline approximation of the chroma profile, (center) the derived gradient magnitude, and (bottom) the derived curvature magnitude. Horizontal lines show the thresholds used to isolate the cusps and inflection points, which are represented by the vertical lines overlaid on the chroma profile. Bullet symbols (●) highlight the inclusion of numeric artifacts among the derived inflection points.

representativeness of the resulting indicators. These problems are only exacerbated when noise is introduced into the derivation process, such as with the Kindlmann color map.

We opted to manually remove any spurious indicators linked to numeric or noise-based artifacts. Figure 3 shows our proposed indicator sets before and after this manual removal. The specific smoothing and thresholding parameters used to derive the indicator sets shown in Figure 3 can be found in Table 1. The archive containing this document also includes a jupyter notebook<sup>†</sup> that contains an interactive tool for exploring the impact of varying these smoothing and thresholding parameters (see Figure 4).

In order to maintain a high level of accuracy in our derived indicator sets, we attempted to minimize the amount of smoothing performed in each indicator set derivation. Differences in the amount of smoothing across indicators sets, however, may result in slight variations in the locations of indicators that should be coincident. A notable example of this can be seen in 4 nearly coincident cusps across the chroma and hue profiles of the Kindlmann color map (marked in 3b). The offsets among these 4 indicators is a constant amount (+/- 0.00392), which sensitivity analysis suggests is tied directly to the difference in  $\sigma$  values. Given the very small orders of magnitude involved, we did not conduct a complete sensitivity analysis of all indicators, but we argue this validates our decision to minimize smoothing to improve accuracy wherever possible.

Color Map	Indicator	Profile	$\sigma$	$\tau$
Traditional	Cusps	L*	0	90000
Traditional	Cusps	C*	0	37000
Traditional	Inflection Points	L*	0.6	295
Traditional	Inflection Points	C*	1.0	135
Traditional	Inflection Points	h	0	3
Jet	Cusps	L*	0	60000
Jet	Cusps	C*	0	80000
Jet	Cusps	h	0	990
Jet	Inflection Points	L*	1.2	158
Jet	Inflection Points	C*	0.8	100
Jet	Inflection Points	h	1.0	6
Kindlmann	Cusps	C*	1.3	18000
Kindlmann	Cusps	h	1.7	270
Kindlmann	Inflection Points	C*	1.5	370
Kindlmann	Inflection Points	h	2.5	3.4

**Table 1:** Gaussian smoothing ( $\sigma$ ) and thresholding ( $\tau$ ) parameters used to derive each set of cusps and inflection points.

<sup>†</sup> For details on how to run the jupyter notebook, see the archive README.

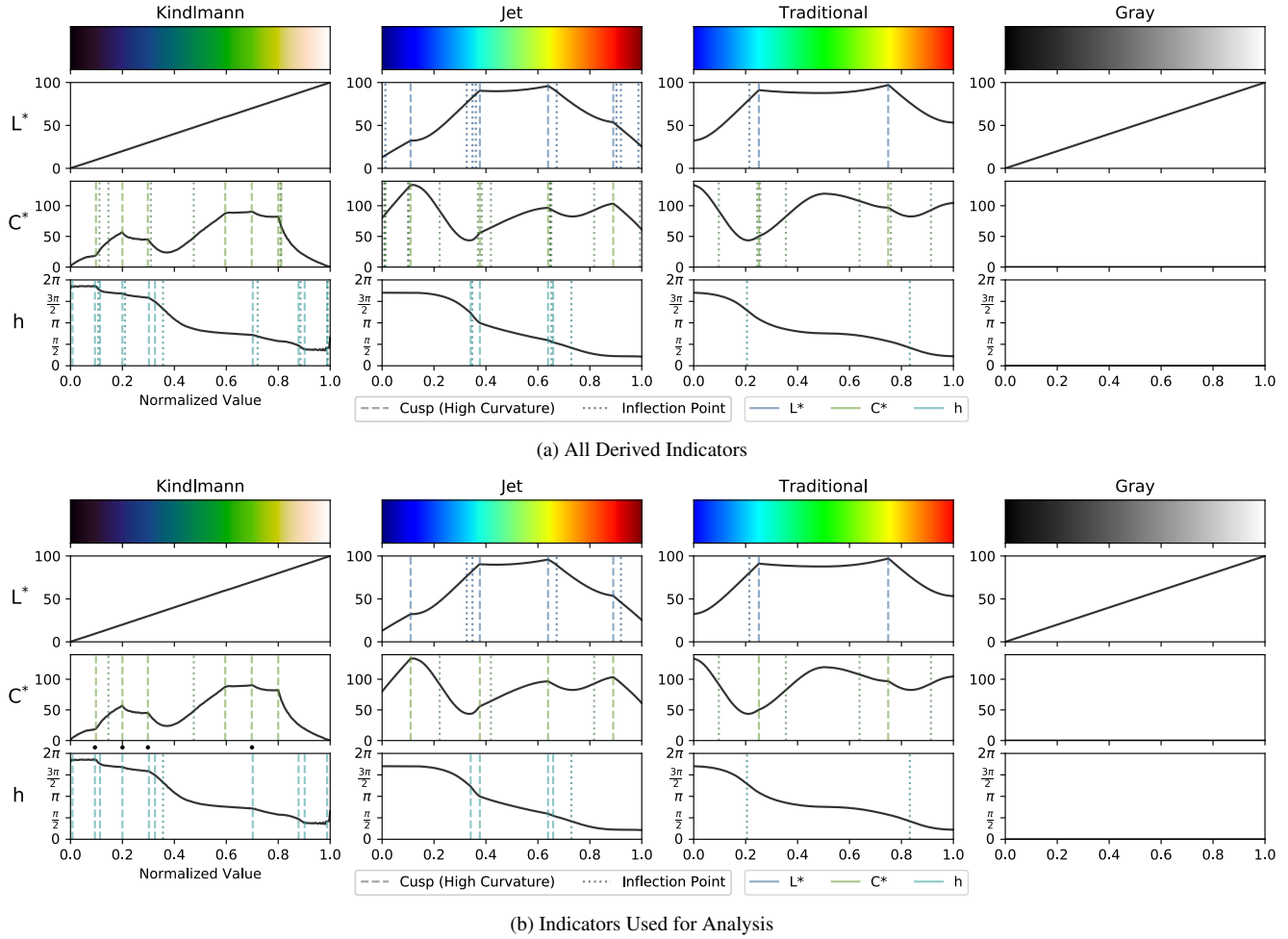


**Figure 3:** A comparison of the original sets of indicators derived using the smoothing and thresholding parameters in Table 1 vs. the indicator sets we wound up using in our analysis. Bullet symbols ( $\bullet$ ) mark 4 nearly coincident indicators across the Kindlmann chroma and hue profiles. The offset appears to be explained by differences in the smoothing parameters used between the indicator sets.

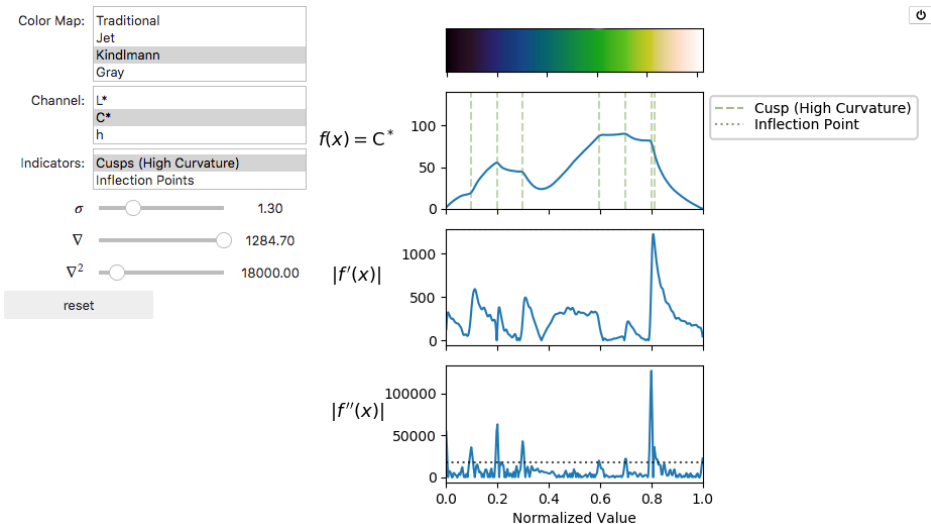


**Figure 4:** An interactive tool for exploring the smoothing and thresholding parameter spaces for finding cusps and inflection points in the CIELCh profiles of each color map in our study.

### C. Kernel Density Estimates and Dependent Data

Kernel density estimation (KDE) is a non-parametric method for estimating the probability density function  $f(x)$  for some random variable  $X$ . KDE is considered a fundamental data-smoothing problem where inferences about a population are made based on a finite data sample. It is widely used in inference procedures across fields such as machine learning [BCM\*13], signal processing [BPR04], data mining [Agg07], and econometrics [ZD12].

An implementation of KDE requires the selection of a suitable kernel weight function, the selection of an appropriate *bandwidth* tuning parameter, and representatively sampled data [ZD12]. A suitable kernel weight function can often easily be selected by relying on one of a handful of widely used kernels: uniform, Gaussian, Epanechnikov, biweight, and triweight [ZD12]. The selection of an appropriate bandwidth, on the other hand, is often more involved.

In many cases, a reasonable bandwidth can be selected manually by simply by looking at the density estimates produced by a range of bandwidths [ZD12], which is roughly analogous to performing a sensitivity analysis. However, a wide range of automatic bandwidth selection mechanisms also exist, some of which are even theoretically optimal given the appropriate set of assumptions [Loa99].

One of the major assumptions associated with optimal bandwidth selection is that underlying data samples are independent and identically distributed (i.i.d.) [AC10]. The participant delimiter placements collected during our study, however, likely fail to meet this assumption. In Section 4.5 of our paper, we highlight that Smeulders et al. show that the placement of black line delineations in a diffracted spectrum change the number of distinct colors perceived, which leads to the placement of additional delineations [SCA94]. We also experienced a similar phenomenon in our early experimental prototypes, suggesting that a given participant's delimiter placements are dependent on one another, with the positions of antecedent delimiters affecting the placement of subsequent delimiters.

For cross-validation (CV) approaches to selecting an optimal bandwidth, however, the i.i.d. assumption is likely overly conservative. For CV, what is important is that the test and training datasets are independent, with the individual samples in both datasets stemming from the same underlying distribution [VRE\*17, SLJ\*17]. Samples within the test and training datasets, however, can have dependencies [SLJ\*17]. Under these relaxed assumptions, *leave-subject-out/leave-cluster-out* CV approaches have also been shown to possess theoretic optimality [XH12].

Because we expect dependencies only among a given subject's delimiter placements, a leave-subject-out CV approach is entirely appropriate for analyzing our experimental data. In keeping with recommended practices, we used a 90%:10% test-train split, and we employed a repeated Monte-Carlo CV strategy to keep the number of folds large given our relatively small sample sizes [RBC\*17, SLJ\*17, LVS\*17]. The jupyter notebook accompanying this document (see the README for details) also includes an interactive tool that allows users to directly explore the sensitivity of the kernel density estimates in our paper by varying a fixed bandwidth. We are not including a proper sensitivity analysis, however, since leave-subject-out CV provides a stronger argument for our bandwidth selections.

## D. Descriptive Statistical Analysis (Expanded)

As stated in Section 5.1 of the paper, we conducted a linear mixed-effects analysis because we employed mixed design with unbalanced sample sizes. Participants were modeled as a random effect, and color map (traditional, grayscale, jet, Kindlmann), dataset (1D, 2D, complex), instruction condition (category, boundary), response method (counted, placed), and potential color-map:dataset and instruction:response-method interactions were all modeled as fixed effects. Additionally, the grayscale color map and complex dataset were used as reference groups, given that we hypothesized differences compared to these groups.

An R Markdown file containing all of the code and resulting model outputs is included in the archive containing this document (see the README for details). Here, we provide a detailed null hypothesis significance testing (NHST) style summary of the findings.

The linear mixed-effects model revealed that each of the rainbow color maps elicited significantly more delineations than grayscale (traditional  $M = 6.29$ ,  $SD = 1.74$ ,  $t(275.01) = 5.19$ ,  $p < .001$ ; jet  $M = 7.83$ ,  $SD = 2.75$ ,  $t(275.01) = 9.41$ ,  $p < .001$ ; Kindlmann  $M = 7.06$ ,  $SD = 2.98$ ,  $t(275.01) = 6.77$ ,  $p < .001$ ; grayscale  $M = 4.85$ ,  $SD = 3.07$ ). Furthermore, the 1D dataset elicited significantly more delineations than the complex dataset (1D  $M = 6.67$ ,  $SD = 3.12$ ; complex  $M = 6.18$ ,  $SD = 2.46$ ) ( $t(275.01) = 1.96$ ,  $p < .049$ ). Although main effects did not reveal a significant difference between the 2D and complex datasets ( $t(275.01) = -1.61$ ,  $p = .106$ ), the analysis did show significant interactions between some of the color maps and the 2D vs. complex datasets. In particular, we found significant interactions between the grayscale and jet color maps for the 2D vs. complex datasets ( $t(275.01) = 4.79$ ,  $p < .001$ ), as well as between the grayscale and Kindlmann color maps for the 2D vs. complex datasets ( $t(275.01) = 3.40$ ,  $p < .001$ ).

To evaluate these interactions, we ran the previously described model on the grayscale, jet, and Kindlmann color maps separately. Post hoc analysis revealed that, for both the jet and Kindlmann color maps, participants perceived significantly more boundaries for the 2D dataset (jet  $M = 8.52$ ,  $SD = 2.70$ ; Kindlmann  $M = 7.35$ ,  $SD = 2.73$ ), compared to the complex dataset (jet  $M = 7.21$ ,  $SD = 2.30$ ,  $t(275.9) = 7.55$ ,  $p < .001$ ; Kindlmann  $M = 6.54$ ,  $SD = 2.85$ ,  $t(275.9) = 4.47$ ,  $p < .001$ ). The grayscale color map, however, did not show a significant difference between the 2D ( $M = 4.41$ ,  $SD = 3.36$ ) and complex ( $M = 4.82$ ,  $SD = 2.08$ ) datasets ( $t(276.01) = -1.67$ ,  $p = 0.96$ ).

These findings support the idea that both the color map and the dataset characteristics influence how people perceive color categories/boundaries in a color-mapped visualization. As discussed in Section 5.1 of the paper, however, these conclusions need to be contextualized by an understanding of the distribution of those perceived boundaries.

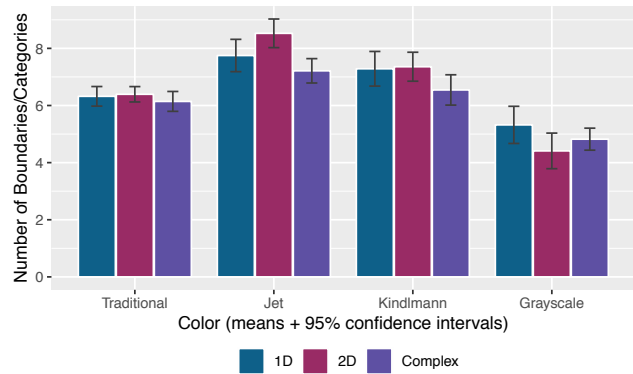


**Figure 5:** A reproduction of Figure 7 from the paper, which shows the mean number of delineations that participants perceived and/or placed along with the 95% confidence interval for each color map and dataset.

## E. Results Overview (Expanded)

This appendix includes both an expanded discussion of observed patterns in participants' responses for the grayscale stimuli and a comprehensive overview of participants' delimiter placements compared against our anticipated indicators.

### Grayscale

Going through the survey responses, we noted multiple cases where participants mentioned using "lines" in the 1D grayscale stimulus to place delimiters. Looking closely at that experimental stimulus, we verified the existence of artifacts that, indeed, look like vertical lines. We were initially concerned that we may have introduced some sort of error when generating the color map, but we were able to verify that the artifacts are inherent to all 24-bit RGB representations of a perceptual grayscale color map. We even verified that the same artifacts exist in versions of the perceptual grayscale color map derived and made available by others [Kov15].

Because human perception of luminance follows an approximate power function [Ste57], a perceptually corrected grayscale color map represents a non-linear traversal across an RGB color space. When transformed into a standard 24-bit representation of RGB (i.e., [255, 255, 255]), this non-linearity causes some RGB colors to be omitted and others to be doubled. Figure 6 shows the locations of these missing and doubled values on top of a reproduction of the 1D grayscale stimuli. The locations of the missing and doubled values appear to correspond to the locations of the artifacts perceived in the color map. Despite using the same color map, the 2D and complex stimuli do not appear to show similar artifacts. We suspect that the visibility of the artifacts is related to the visual angle subtended by these missing and doubled values, which would also explain why the effect is more noticeable when the 1D stimulus is larger.

In the complex grayscale stimulus, however, we also need to account for *data features* in our analysis of the results. As illustrated in Figure 7, we approximated these features through a small set of isolines. We derived these isolines by using a Canny edge detector to find edges in the original dataset, taking the data values associated with those edge locations, and thresholding the peaks of the resulting probability distribution approximated via KDE (*bandwidth* = 0.05). We felt that the resulting isolines (Figure 7d) reasonably reflect the pronounced features in the dataset.

The full set of participants' delimiter placements across the grayscale stimuli are shown in Figure 8. We provide explicit comparisons against the color map artifacts for the 1D stimuli and against our approximated data features for the complex stimuli. As noted in the paper, the doubled values in the color map correspond to the large cluster of delimiters placed by participants in the lower range of the color map for the 1D stimulus. It is unclear whether the delimiters placed in the mid-to-high range of the color map are tied to the missing values in the color map or not. For the complex stimuli, the approximated data features correspond to large clusters of participants' placed delimiters. In general, these clusters have more variability than the clusters associated with the perceived bands in the rainbow color maps. This added variability could be due to the fact that isolines are loose approximations of the edges we detect in the data (compare Figures 7a and 7d).

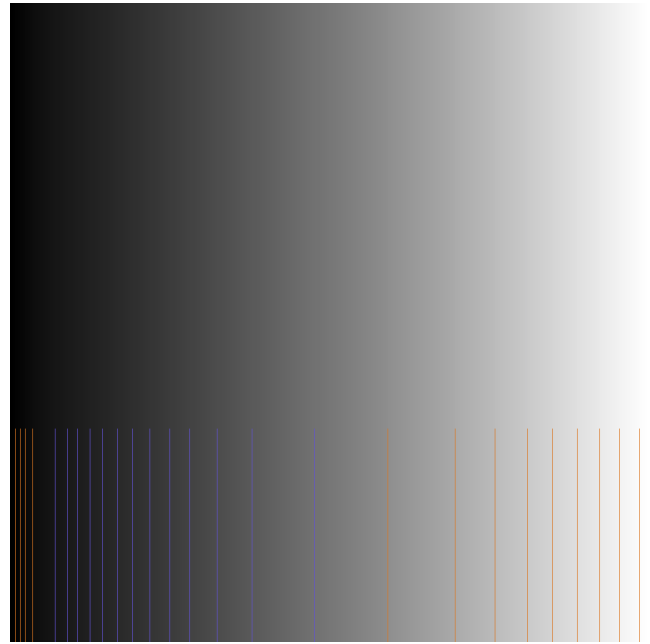


**Figure 6:** Visible artifacts in the 1D grayscale stimuli match the locations of missing (red) and doubled (blue) values inherent to the perceptual grayscale color map. The effect is more pronounced at larger sizes, such as the size used in the experiment.

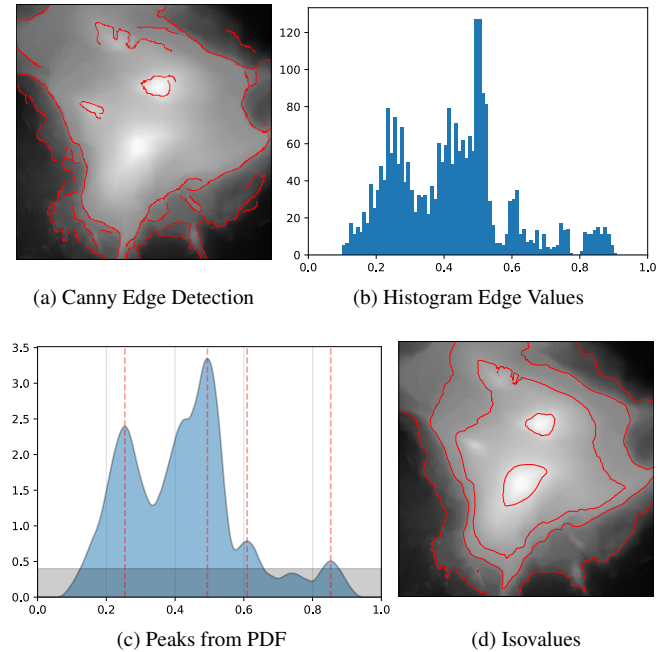


**Figure 7:** Approximating features in the complex dataset. We first (a) ran a Canny edge detector. We then (b) took the data values associated with those edge locations and (c) found the peaks from a kernel density estimate (KDE) of the probability distribution for those edge values. After thresholding, the resulting peaks provided (d) a set of isolines that reflect the underlying data features.

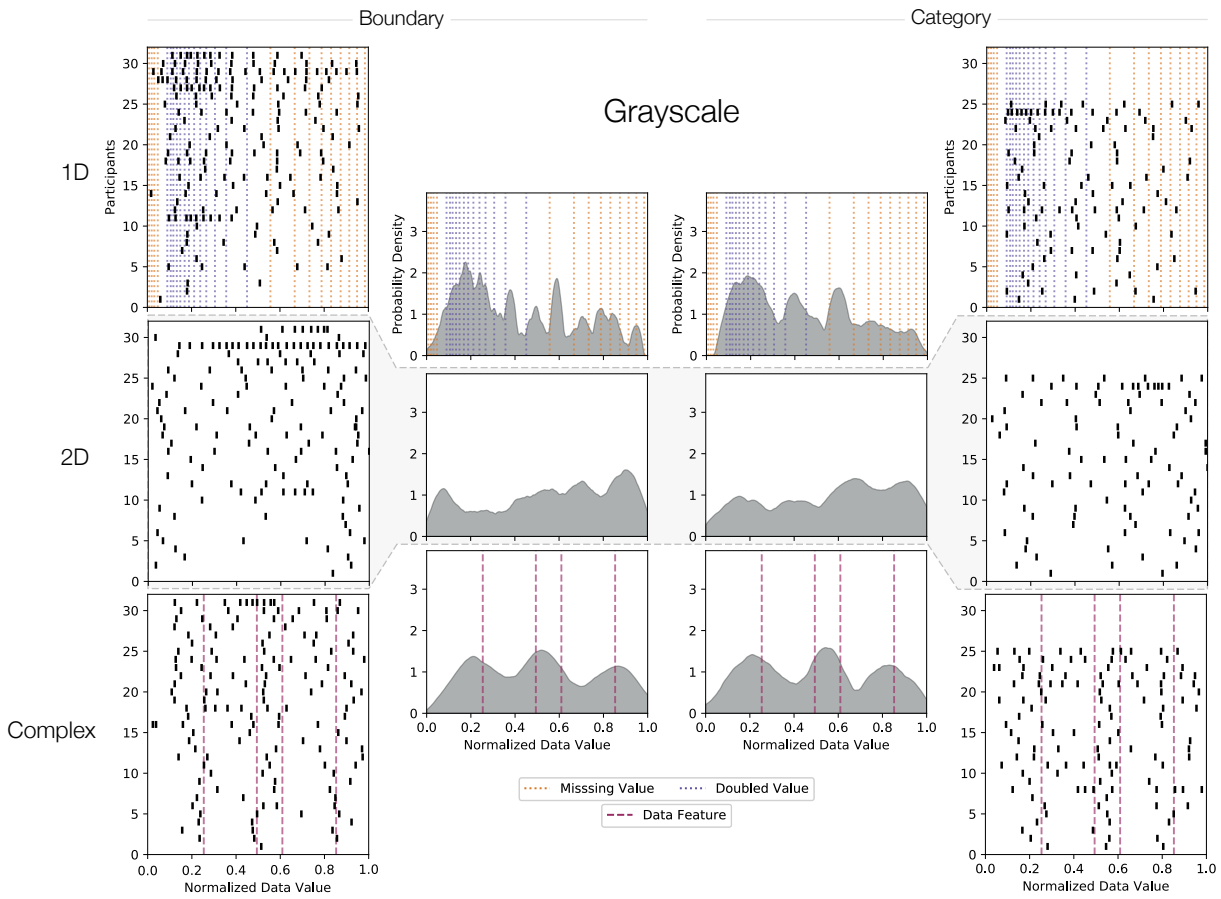


**Figure 8:** The complete set of participant delimiters placements for the grayscale color map. The three rows contain the delimiters associated with the 1D, 2D, and complex stimuli, respectively. Each row shows both the individual boundaries placed by each participant in that stimuli and the probability distribution function computed from all boundaries placed in that stimuli. Responses from the boundary condition are on the left, and responses from the category condition are on the right.

### **Rainbow Color Maps**

The following pages show the full sets of participants' delimiter placements associated with the three different rainbow color maps in the study. These expanded results show the same general patterns outlined in the paper. The results show consistency in where color boundaries/categories are perceived and placed across participants. The distributions of participants' responses are similar across the instruction conditions. Many of the trends or clusters in participants' delimiter placements do appear to correspond to cusps and/or inflection points in the perceptual dimensions of color for each color map. Additionally, the results show pronounced shifts across the different datasets for a given color map, including between the 1D and 2D stimuli. Finally, as any trends associated with the approximated complex dataset features also appear to be present in the 1D and 2D stimuli, the results provide no conclusive evidence that the data features in the complex dataset had any significant effect on participants' responses.

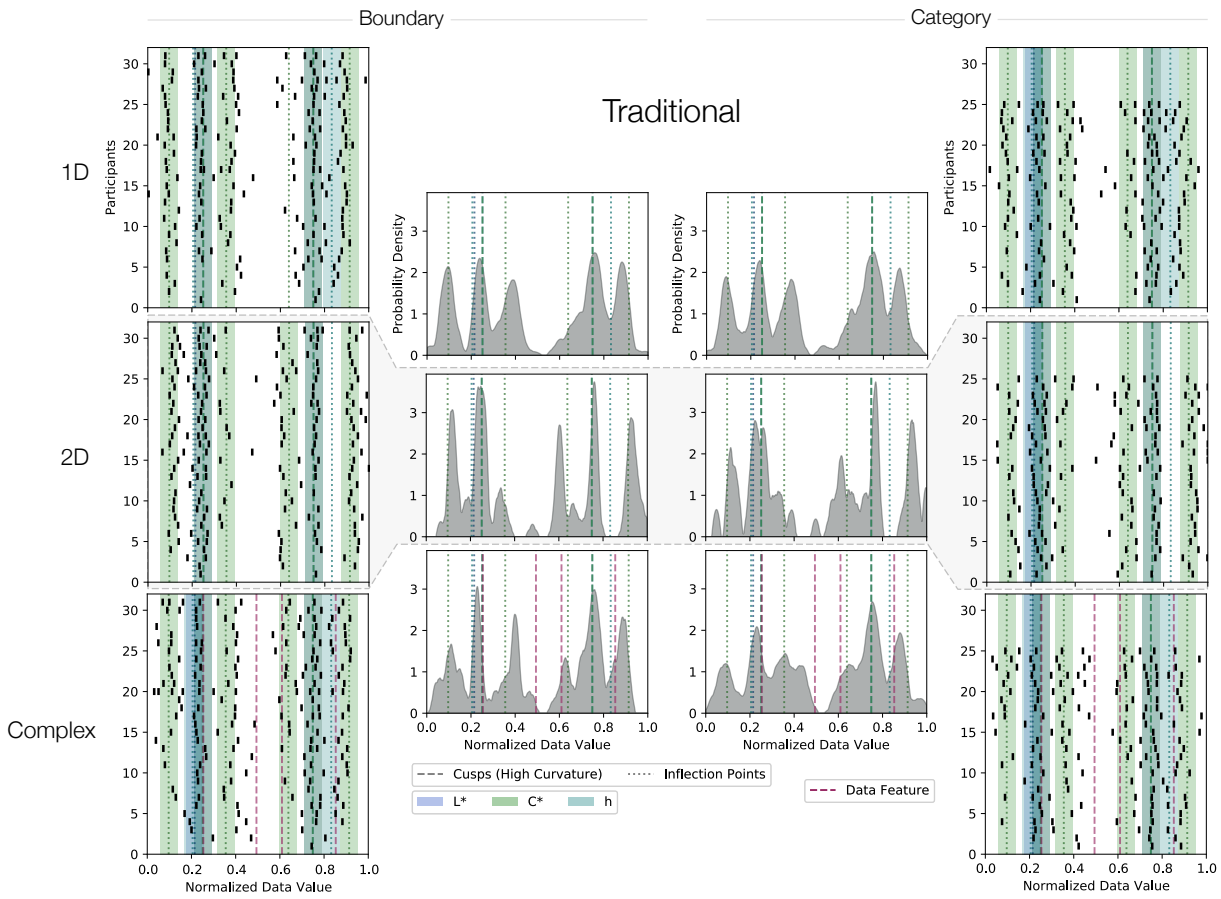


**Figure 9:** The complete set of participant delimiters placements for the traditional rainbow color map. The three rows contain the delimiters associated with the 1D, 2D, and complex stimuli, respectively. Each row shows both the individual boundaries placed by each participant in that stimuli and the probability distribution function computed from all boundaries placed in that stimuli. Responses from the boundary condition are on the left, and responses from the category condition are on the right.

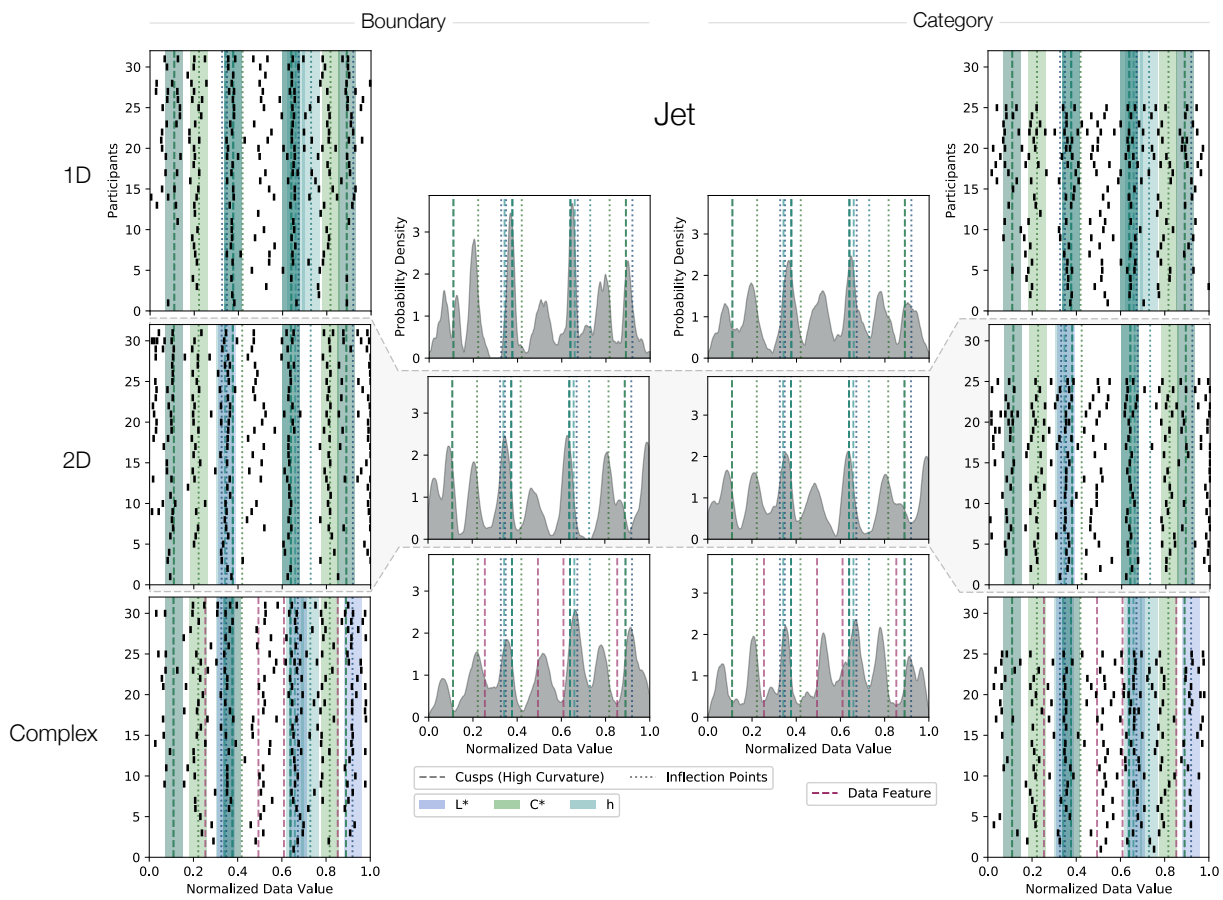


**Figure 10:** The complete set of participant delimiters placements for the jet color map. The three rows contain the delimiters associated with the 1D, 2D, and complex stimuli, respectively. Each row shows both the individual boundaries placed by each participant in that stimuli and the probability distribution function computed from all boundaries placed in that stimuli. Responses from the boundary condition are on the left, and responses from the category condition are on the right.

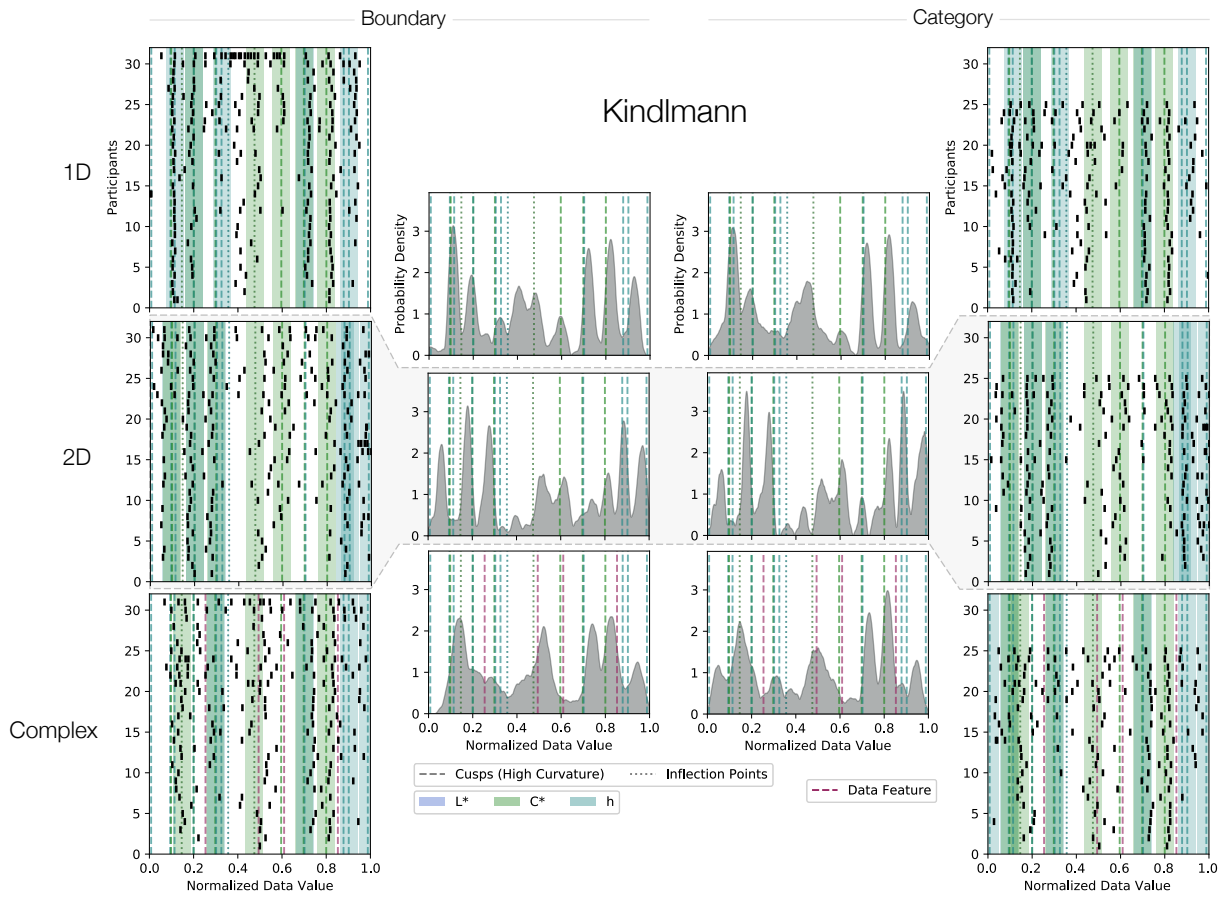


**Figure 11:** The complete set of participant delimiters placements for the Kindlmann color map. The three rows contain the delimiters associated with the 1D, 2D, and complex stimuli, respectively. Each row shows both the individual boundaries placed by each participant in that stimuli and the probability distribution function computed from all boundaries placed in that stimuli. Responses from the boundary condition are on the left, and responses from the category condition are on the right.

## References

- [AC10] ARLOT S., CELISSE A.: A survey of cross-validation procedures for model selection. *Statistics Surveys* 4 (2010), 40–79. doi: [10.1214/09-SS054](https://doi.org/10.1214/09-SS054). 5
- [Agg07] AGGARWAL C. C.: On Density Based Transforms for Uncertain Data Mining. In *2007 IEEE 23rd International Conference on Data Engineering* (Apr. 2007), pp. 866–875. doi: [10.1109/ICDE.2007.367932](https://doi.org/10.1109/ICDE.2007.367932). 5
- [BCM\*13] BIGGIO B., CORONA I., MAIORCA D., NELSON B., ŠRNĐIĆ N., LASKOV P., GIACINTO G., ROLI F.: Evasion Attacks against Machine Learning at Test Time. In *Machine Learning and Knowledge Discovery in Databases* (2013), Blockeel H., Kersting K., Nijsen S., Železný F., (Eds.), Lecture Notes in Computer Science, Springer Berlin Heidelberg, pp. 387–402. 5
- [BPR04] BOSCOLO R., PAN H., ROYCHOWDHURY V. P.: Independent component analysis based on nonparametric density estimation. *IEEE Transactions on Neural Networks* 15, 1 (Jan. 2004), 55–65. doi: [10.1109/TNN.2003.820667](https://doi.org/10.1109/TNN.2003.820667). 5
- [CZC\*18] CHEN J., ZHANG G., CHIOW W., LAIDLAW D. H., AUCHUS A. P.: Measuring the Effects of Scalar and Spherical Colormaps on Ensembles of DMRI Tubes. *arXiv:1810.07882 [cs]* (Oct. 2018). arXiv: [1810.07882](https://arxiv.org/abs/1810.07882). 2
- [DPR\*18] DASGUPTA A., POCO J., ROGOWITZ B., HAN K., BERTINI E., SILVA C. T.: The Effect of Color Scales on Climate Scientists’ Objective and Subjective Performance in Spatial Data Analysis Tasks. *IEEE Transactions on Visualization and Computer Graphics* (2018), 1–1. doi: [10.1109/TVCG.2018.2876539](https://doi.org/10.1109/TVCG.2018.2876539). 2
- [Gre11] GREEN D. A.: A colour scheme for the display of astronomical intensity images. *Bulletin of the Astronomical Society of India* 39 (June 2011), 289–295. arXiv: [1108.5083](https://arxiv.org/abs/1108.5083). 2
- [KC01] KINCAID D. R., CHENEY E. W.: *Numerical Analysis: Mathematics of Scientific Computing*, 3 edition ed. Brooks Cole, Pacific Grove, CA, Oct. 2001. 3
- [Kov15] KOVESI P.: Good Colour Maps: How to Design Them. *arXiv:1509.03700 [cs]* (Sept. 2015). arXiv: [1509.03700](https://arxiv.org/abs/1509.03700). 7
- [KRC02] KINDLMANN G., REINHARD E., CREEM S.: Face-based Luminance Matching for Perceptual Colormap Generation. In *Visualization, 2002. VIS ’02.* (Nov. 2002), pp. 299–306. doi: [10.1109/VISUAL.2002.1183788](https://doi.org/10.1109/VISUAL.2002.1183788). 2
- [Loa99] LOADER C. R.: Bandwidth selection: Classical or plug-in? *The Annals of Statistics* 27, 2 (Apr. 1999), 415–438. doi: [10.1214/aos/1018031201](https://doi.org/10.1214/aos/1018031201). 5
- [LVS\*17] LITTLE M. A., VAROQUAUX G., SAEB S., LONINI L., JAYARAMAN A., MOHR D. C., KORDING K. P.: Using and understanding cross-validation strategies. Perspectives on Saeb et al. doi: [10.1093/gigascience/gix020](https://doi.org/10.1093/gigascience/gix020). 5
- [Mor16] MORELAND K.: Why We Use Bad Color Maps and What You Can Do About It. *Electronic Imaging 2016*, 16 (Feb. 2016), 1–6. doi: [10.2352/ISSN.2470-1173.2016.16.HVEI-133](https://doi.org/10.2352/ISSN.2470-1173.2016.16.HVEI-133). 2
- [Nic12] NICCOLI M.: The Rainbow is Dead... Long Live the Rainbow! - Perceptual Palettes, Part 5 - CIE Lab Linear L\* Rainbow. <https://mycarta.wordpress.com/2012/12/06/the-rainbow-is-deadlong-live-the-rainbow-part-5-cie-lab-linear-l-rainbow/>, June 2012. 2
- [RBC\*17] ROBERTS D. R., BAHN V., CIUTI S., BOYCE M. S., ELITH J., GUILLERA-ARROTA G., HAUENSTEIN S., LAHOZ-MONFORT J. J., SCHRÖDER B., THUILLER W., WARTON D. I., WINTLE B. A., HARTIG F., DORMANN C. F.: Cross-validation strategies for data with temporal, spatial, hierarchical, or phylogenetic structure. 913–929. doi: [10.1111/ecog.02881](https://doi.org/10.1111/ecog.02881). 5
- [SCA94] SMEULDERS N., CAMPBELL F. W., ANDREWS P. R.: The role of delineation and spatial frequency in the perception of the colours of the spectrum. *Vision Research* 34, 7 (Apr. 1994), 927–936. doi: [10.1016/0042-6989\(94\)90041-8](https://doi.org/10.1016/0042-6989(94)90041-8). 5
- [SLJ\*17] SAEB S., LONINI L., JAYARAMAN A., MOHR D. C., KORDING K. P.: The need to approximate the use-case in clinical machine learning. doi: [10.1093/gigascience/gix019](https://doi.org/10.1093/gigascience/gix019). 5
- [Ste57] STEVENS S. S.: On the psychophysical law. *Psychological Review* 64, 3 (May 1957), 153–181. 7
- [STP17] SUMMA B., TIERNY J., PASCUCCI V.: Visualizing the Uncertainty of Graph-based 2D Segmentation with Min-path Stability. *Computer Graphics Forum* 36, 3 (2017), 133–143. doi: [10.1111/cgf.13174](https://doi.org/10.1111/cgf.13174). 2
- [Sza18] SZAFIR D. A.: Modeling Color Difference for Visualization Design. *IEEE Transactions on Visualization and Computer Graphics* 24, 1 (Jan. 2018), 392–401. doi: [10.1109/TVCG.2017.2744359](https://doi.org/10.1109/TVCG.2017.2744359). 2
- [VRE\*17] VAROQUAUX G., RAAMANA P. R., ENGEMANN D. A., HOYOS-IDROBO A., SCHWARTZ Y., THIRION B.: Assessing and tuning brain decoders: Cross-validation, caveats, and guidelines. 166–179. doi: [10.1016/j.neuroimage.2016.10.038](https://doi.org/10.1016/j.neuroimage.2016.10.038). 5
- [War88] WARE C.: Color Sequences for Univariate Maps: Theory, Experiments and Principles. *IEEE Computer Graphics and Applications* 8, 5 (Sept. 1988), 41–49. doi: [10.1109/38.7760](https://doi.org/10.1109/38.7760). 2
- [XH12] XU G., HUANG J. Z.: Asymptotic optimality and efficient computation of the leave-subject-out cross-validation. *The Annals of Statistics* 40, 6 (Dec. 2012), 3003–3030. doi: [10.1214/12-AOS1063](https://doi.org/10.1214/12-AOS1063). 5
- [YLL15] YOO M.-J., LEE I.-K., LEE S.: Color Sequence Preserving Decolorization. *Computer Graphics Forum* 34, 2 (2015), 373–383. doi: [10.1111/cgf.12567](https://doi.org/10.1111/cgf.12567). 2
- [ZD12] ZAMBOM A. Z., DIAS R.: A Review of Kernel Density Estimation with Applications to Econometrics. *arXiv:1212.2812 [stat]* (Dec. 2012). arXiv: [1212.2812](https://arxiv.org/abs/1212.2812). 5
- [ZH16] ZHOU L., HANSEN C. D.: A Survey of Colormaps in Visualization. *IEEE Transactions on Visualization and Computer Graphics* 22, 8 (Aug. 2016), 2051–2069. doi: [10.1109/TVCG.2015.2489649](https://doi.org/10.1109/TVCG.2015.2489649). 2